Information Fusion

BCINet: Bilateral Cross-Modal Interaction Network for Indoor Scene Understanding in RGB-D Images

--Manuscript Draft--

Manuscript Number:	INFFUS-D-22-00538R1
Article Type:	Research paper
Keywords:	Scene understanding; RGB-D; bilateral cross-modal interaction; hybrid pyramid dilated convolution; deep learning
Abstract:	Depth cue has proven to be useful information in the indoor scene understanding of RGB-D images for providing a geometric counterpart to RGB representation. However, because of the differences between RGB-D image pairs, utilizing cross-modal data effectively is a key issue. Most methods exclusively leverage depth data to unilaterally complement RGB data for better feature representation; they invariably ignore the fact that RGB and depth data can bilaterally complement each other. Herein, a novel RGB-D scene-understanding network called BCINet is presented, in which RGB and depth data bilaterally complement each other via a proposed bilateral cross-modal interaction module (BCIM). The BCIM helps to capture cross-modal complementary cues by crossly fusing enhanced features from one modality to the counterpart modality through a feature enhanced module. Meanwhile, exploiting the long-range dependencies of RGB-D features is also significant for accurate scene understanding. Specifically, we design a hybrid pyramid dilated convolution module to enlarge the receptive fields along both the vertical and horizontal spatial directions to adaptively capture diverse contexts with different shapes. Additionally, we propose a context-guided module to aggregate these diverse higher-level contexts with lower-level features in the encoder to guide the information flow for progressively refining the segmentation map. Experimental results on two indoor scene datasets demonstrate the superiority and effectiveness of the proposed BCINet over several state-of-the-art approaches.

Dear Editors,

Thank you for considering Manuscript ID: INFFUS-D-22-00538. We also thank the reviewers for providing helpful suggestions to improve the quality of the manuscript. We have revised our manuscript according to the reviewers' comments.

This document contains our responses to the reviewers' comments.

Best regards,

Wujie Zhou
Dec. 24, 2022

Response to reviewers

Title: BCINet: Bilateral Cross-Modal Interaction Network for Indoor Scene Understanding in RGB-D Images

Authors: Wujie Zhou, Yuchun Yue, Meixin Fang, Xiaohong Qian, Rongwang Yang, Lu Yu

Response:

We appreciate the reviewers' constructive comments. In the revised manuscript, we made the following improvements:

(1) The reviewer's comments have been considered in the revision.

(2) Some descriptions related to symbols and equations have been rewritten, to improve their clarity.

(3) Some writing errors have been corrected. Meanwhile, the language of the paper has been thoroughly and carefully revised.

(4) The descriptions for some of the references have been clarified.

(5) Proper rationale behind the design of each module have been added in the revised manuscript.

In the following, we have answered each comment in **BOLD** font.

Editor and Reviewer comments:

AE: Please fulfil all the reviewers' minor and major concerns, seriously and carefully.

Moreover, I'd like to see a range of applications/domains profiting from your proposal.

Just an example is here:

Collaborative robotics: Towards Collaborative Robotics in Top View Surveillance: A Framework for Multiple Object Tracking by Detection Using Deep Learning. IEEE CAA J. Autom. Sinica 8(7): 1253-1270 (2021)

IoT: Internet of Things as System of Systems: A Review of Methodologies, Frameworks, Platforms, and Tools. IEEE Trans. Syst. Man Cybern. Syst. 51(1): 223-236 (2021)

Underwater images: An Experimental-Based Review of Image Enhancement and Image Restoration Methods for Underwater Imaging. IEEE Access 7: 140233-140251 (2019)

Response:

Thank you for your comments. In the revised manuscript, above-mentioned references have been added and reviewed in section 1.

[1] Y. Wang, W. Song, G. Fortino, L. -Z. Qi, W. Zhang and A. Liotta, Underwater images: An Experimental-Based Review of Image Enhancement and Image Restoration Methods for Underwater Imaging, IEEE Access, 7, (2019) 140233–140251.

[3] I. Ahmed, S. Din, G. Jeon, F. Piccialli and G. Fortino, Collaborative robotics: Towards Collaborative Robotics in Top View Surveillance: A Framework for Multiple Object Tracking by Detection Using Deep Learning, IEEE CAA J. Autom. Sinica, 8, (2021) 1253–1270.

[5] G. Fortino, C. Savaglio, G. Spezzano and M. Zhou, IoT: Internet of Things as System of Systems: A Review of Methodologies, Frameworks, Platforms, and Tools, IEEE Trans. Syst. Man Cybern. Syst., 51, (2021) 223–236.

Reviewer #1:

# Summary

This paper presents a method named indoor scene understanding from RGBD images. It designs three core components (i.e., BCIM, HPDC, and CGM) to achieve better fusion between two modalities. The results of experiments conducted on the NYUv2 and SUN datasets indicate that the proposed BCINet outperforms existing several RGB-D scene-understanding models. Overall, this manuscript is well-written and -organized. But still, several issues should be considered in next response.

# Weaknesses

-- Several works also study the bidirectional attention mechanism in computer vision, such as [1,2*,3*,4*], which should be discussed in the related works (Section 2.2).*

Response:

Thank you for your comments. In the revised manuscript, above-mentioned references have been added and reviewed in section 2.2 as follows:

"Recently, the bidirectional-attention mechanism has been used for computer vision tasks such as depth estimation [52], object segmentation [53], object classification [54], and image-text matching [55]."

[52] S. Aich, J. M. U. Vianney, M. A. Islam, and M. K. B. Liu, Bidirectional attention network for monocular depth estimation, In 2021 IEEE International Conference on Robotics and Automation (ICRA), (2021) 11746–11752.

[53] G. P. Ji, K. Fu, Z. Wu, D.-P. Fan, J. Shen, and L. Shao, Full-duplex strategy for video object segmentation. In Proceedings of the IEEE/CVF International Conference on Computer Vision, (2021) 4922–4933.

[54] C. Liu, H. Xie, Z. Zha, L. Yu, Z. Chen, and Y. Zhang, Bidirectional attention-recognition model for fine-grained object classification. IEEE Transactions on Multimedia, 22(7), (2019) 1785–1795.

[55] C. Liu, Z. Mao, A. A. Liu, T. Zhang, B. Wang, and Y. Zhang, Focus your attention: A bidirectional focal attention network for image-text matching. In Proceedings of the 27th ACM International Conference on Multimedia, 2019, pp. 3–11.

-- Lack qualitative results on NYUv2 and SUN RGBD datasets

Response:

Sorry for our simple description. In the revised manuscript, qualitative comparison have been added, and is shown as follows:

3) Qualitative Comparison

To further demonstrate the predicted performance of the proposed BCINet, we conducted qualitative scene-understanding analyses by comparing BCINet with other methods [29, 31, 36, 48] and presented the scene-understanding results for a variety of indoor RGB-D images. Figure 7 shows the scene-understanding maps for RGB-D scenes obtained using NYUDv2, where BCINet obtained more accurate scene-understanding maps regardless of similar scenes or object size. Furthermore, the difference between similar categories is clearer. From these comparisons, we can conclude that BCINet not only accurately located the scene-understanding categories but also acquired detailed cues to recognize smooth objects.

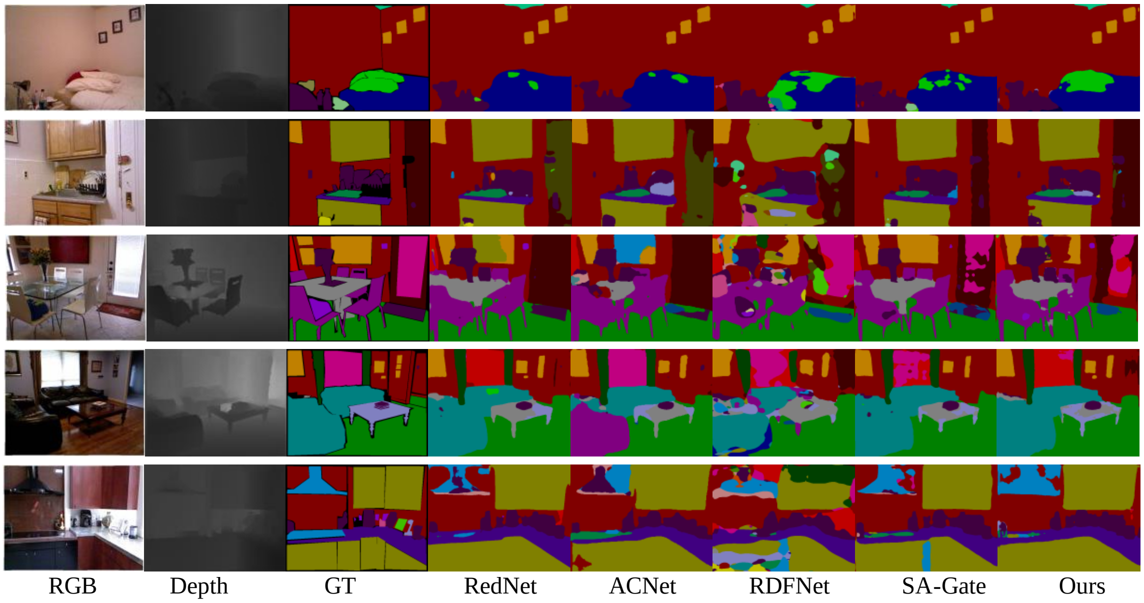

Fig. 7. Scene-understanding maps for RGB-D indoor scenes.

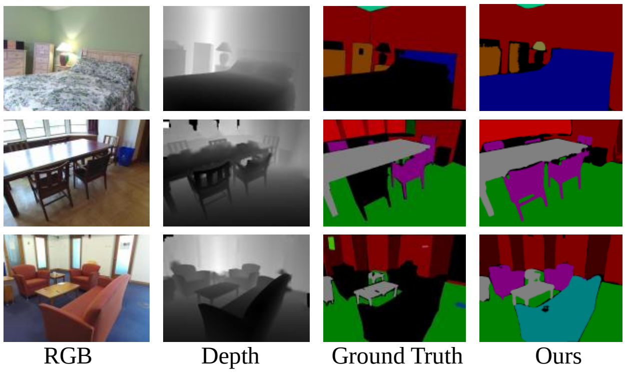

Fig. 8. Scene-understanding results from RGB-D images of the SUN test set.

Fig. 8 shows the scene-understanding results for RGB-D images using SUN. Some objects in SUN are mistakenly labeled as void, which is the background. Conversely, BCINet satisfactorily distinguishes such objects and shows good generalization. As shown in Fig. 8, some mistakes when labelling beds, chairs, and sofas exist. BCINet can correctly recognize these wrongly labeled objects using the information learned from other correctly labeled objects, demonstrating the superior performance of BCINet regarding complex objects and scenes.

-- *Could the authors provide more efficiency comparisons (flops and fps) among existing competing methods?*

Response:

Thank you for your suggestions. In the revised manuscript, complexity evaluation has been added in Section 4.4 as follows:

4.4 Complexity Evaluation

Since runtime is an essential indicator of algorithm performance, we evaluated BCINet under the same conditions. We considered network inference time, number of floating-point operations, and parameter capacity as BCINet efficiency indicators—denoted as FPS, FLOPS, and Params, respectively.

To verify BCINet efficiency, we conducted extensive experiments and comparisons with SOTA RedNet [29], ACNet [48], RDFNet [31] and SA-Gate [36] models, as listed in Table 3. Therefore, the proposed BCINet is

concluded to be an efficient network suitable for real-time applications.

Table 3. Efficiency measures on NYUv2 test set. FPS, FLOPS (G), and Params (M) represent network inference time, number of floating-point operations, and parameter capacity, respectively.

Models	Parameter(M)↓	FPS↑	Flops(G)↓
RedNet (ResNet50) [29]	82.0	26.5	101.8
ACNet (ResNet50) [48]	116.6	21.2	126.3
RDFNet (ResNet101) [31]	443.8	11.4	648.7
SA-Gate (ResNet101) [36]	110.6	16.6	176.5
Ours (ResNet50)	78.38	27.3	97.30

-- *Could the proposed method be applied to outdoor RGBD scene understanding tasks?*

Response:

Thank you for your comments. Through extensive literature review, the outdoor RGBD scene understanding datasets are not released.

In the future, we will continue improving BCINet and attempt to apply it to other computer vision tasks, such as outdoor RGB-D crowd counting and RGB-thermal scene-understanding.

Minor issues:

-- *The best performance should be bolded in the tables for better readability.*

Response:

Thank you for your suggestion. In the revised manuscript, the best performance has been highlighted in the tables for better readability.

[1] Bidirectional Attention Network for Monocular Depth Estimation*

[2] Full-duplex strategy for video object segmentation*

[3] Bidirectional Attention-Recognition Model for Fine-Grained Object Classification*

[4] Focus your attention: A bidirectional focal attention network for image-text matching*

Reviewer #2:

This paper addresses the RGB-D semantic segmentation by interacting cross-modality features with several carefully designed modules: 1) In BCIM module, cross-modality feature is distilled by an FEM with a series of pooling operations to enhance the counterpart unimodal feature representation learning, and 2) HPDC is designed by using different sizes of dilation rate to overcome the shortages of ASPP module.

Paper strength:

1) The paper is well written making the motivation clear.

2) The results are reasonably good.

Response:

Thank you for your comments.

Paper weakness:

1) The ablation study only removes each proposed module to verify the final segmentation results which is not enough to support the insight of this paper. It's strongly encouraging to investigate the effectiveness that the proposed modules are specially and explicitly explored for bilateral cross-modality representation learning enhancement instead of only showing a final segmentation result. Several suggestions are as follows.

a) A baseline with self-attention based modules to enhance the unimodal representation learning should be added to validate the effectiveness of BCIM module on transferring cross-modality information.

Response:

Thank you for your suggestion. In the revised manuscript, a baseline with self-attention based modules to enhance the unimodal representation learning have be added to validate the effectiveness of BCIM module on transferring cross-modality information.

“To validate the effectiveness of BCIM on transferring cross-modality information, a baseline with self-attention-based modules to enhance the unimodal representation learning has been added, as shown in Table 4. Although the experimental results of this method are lower than that of the proposed method, they are very competitive.”

b) RGB and depth data are very different data, which makes the two-stream framework prevalent in RGB-D related tasks, since it's easier to learning better modality-specific features for CNN architectures than directly learning the RGB-D representation by shared weights. However, in this paper, the layer-wise modality-specific features are selectively fused for unimodal representation learning. SO, i'm curious to know:

i) how each modality-specific branch performs on each modality-specific data and cross-modality data in the proposed method;

Response:

Thank you for your comments. In the revised manuscript, to validate the cross-modality data in the proposed method, we only reconstructed the RGB branch. This method only uses single mode features (without BCIM), and the experimental results are not particularly good.

ii) What's the difference if we concatenate the two inputs and feed it to a self-attention based semantic segmentation task;

Response:

We apologize for the simple description given. We have included the following detailed descriptions in the revised manuscript:

“To validate the effectiveness of BCIM on transferring cross-modality information, a baseline with

self-attention-based modules to enhance the unimodal representation learning has been added, as shown in Table 4. Although the experimental results of this method are lower than that of the proposed method, they are very competitive.”

iii) the visualization of learned modality-specific weights to help demonstrate the novelty and effectiveness of the proposed BCIM module.

<u>Response:</u>

Thank you for your comments. In the revised manuscript, the visualization of learned modality-specific weights have been added.

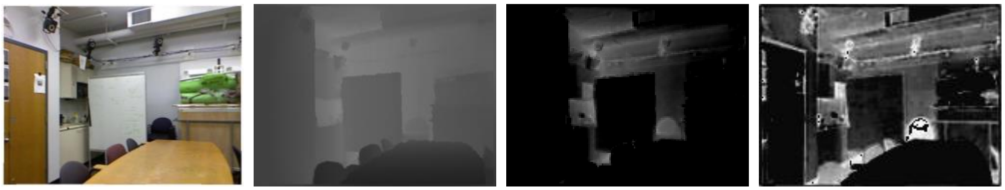

(a) RGB (b) Depth (c) S_i^R (c) S_i^D

Fig. 4 The visualization of learned modality-specific weights

2) Fig.2 is missing, which makes it hard to capture the background on HPDC and CGM modules.

<u>Response:</u>

Sorry for our mistakes. In the revised manuscript, the Fig. 2 has been added, which is shown as follows:

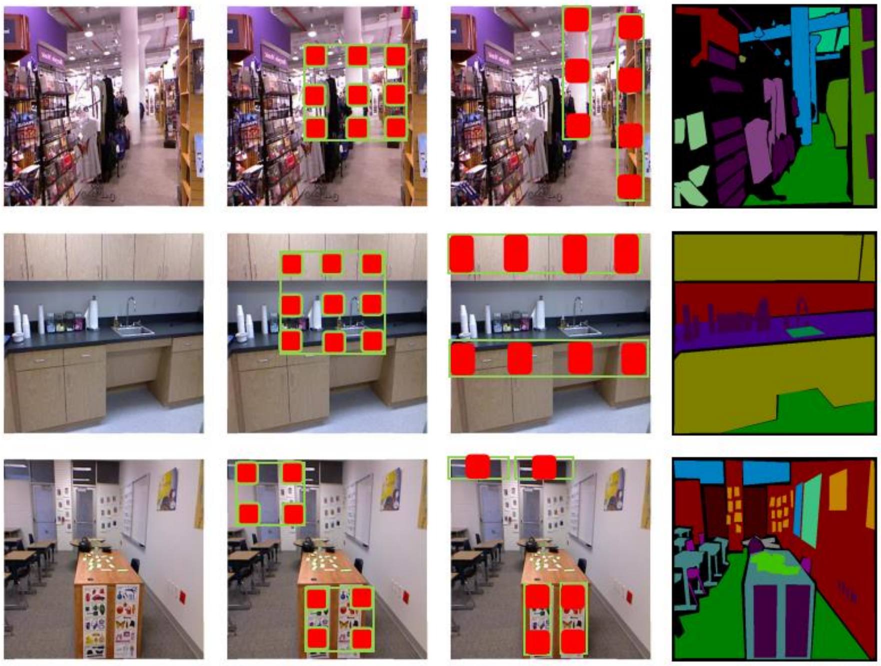

Fig. 2. Illustration of the difference between common dilated convolution and proposed HPDC for scene-understanding. The original RGB image, common dilated convolution operating on RGB, HPDC operating on RGB, and corresponding ground truth are displayed from left to right.

3) In fig.6 and fig.7, though improvement could be found when using the proposed modules, additional mistakes could also be observed, e.g., in the third row of fig.6, the blue stripe area appears over the image without FEM but does not appear without BCIM. In fig.7 the quilt is better parsed with ASPP. It's better to discuss the trade-off between the advantage and shortage of the proposed method.

<u>Response:</u>

Sorry for the lack of explanation. In the revised manuscript, more detailed description and explanation has been added, and is shown as follows:

"2) Effect of BCIM and FEM: **We designed the BCIM to explicitly model the complex relationships between RGB images and depth data by achieving bilateral cross-modal complementary information interaction. When we removed the BCIM from the whole framework, as shown in Table 4, the mIoU fell by 0.9%, verifying the effectiveness of our BCIM. Notably, if the FEM is removed from BCIM, the mIoU falls by 1.41%, which is worse than the results of removal of the whole BCIM. This indicates that inferior performance can result if we simply crossly fuse the original features of both modalities to each other without enhancing the feature correction. This substantiates our argument given in the Introduction and also validates the effectiveness of our FEM. For visualizations, as shown in the 4th column in Fig. 9, without BCIM, the model fails to obtain complementary cues, resulting in some objects with ambiguous appearance not being correctly classified. Additionally, owing to the lack of the FEM, the single modality discriminative features cannot be highlighted and extra noise is introduced, as can be seen in the 5th column. These situations are obviated when BCIM embedded with FEM is applied. <u>In the third row of Fig. 9, although the blue striped area appears over the image without FEM, it does not appear in the one without BCIM, indicating more errors in the segmentation of other regions without FEM.</u>"**

3) Effect of HPDC: **As can be seen in Table 4, the removal of HPDC causes a performance degradation of approximately 3.81%, which means that capturing diverse and anisotropic contexts plays a very important role in learning effective features. To verify the superiority of HPDC compared with the existing ASPP, we ablated HPDC by one more detailed experiment. As displayed in Table 4, when we replace our HPDC with common ASPP, the performance declines by 0.58%, indicating that the three branches that adopt dilated rectangular convolutions in HPDC yield extra gains. <u>As shown in the third row of Fig. 10, although the quilt is better parsed with ASPP, some additional errors in the segmentation of other regions with ASPP exist.</u> As shown in the 4th column in Fig. 10, when HPDC is removed, the model fails to formulate long dependencies and large-scale variations between objects. Furthermore, if the HPDC is replaced by ASPP, objects with irregular shapes cannot be well segmented or correctly classified, which proves the effectiveness of the design of our HPDC."**

4) It seems like ResNet-50 is the only model evaluated. I highly recommend the authors to run the core experiments using other backbones, preferably not ResNet, to demonstrate the generalizability.

<u>**Response:**</u>

Thank you for your suggestion. In the revised manuscript, to validate the influence of the backbone on the proposed BCINet, we have compared the performances of several other popular backbone structures, which are shown as follows:

1) Effect of Backbone: **To verify the influence of the backbone on BCINet, we compared the prediction performances of several other popular backbones (e.g., MobileNetV2, VGG16, and various ResNets with different sizes of parameter). Table 5 shows the experimental results. BCINet (ResNet50) obtained better performance compared with other backbones, indicating that our selection is desirable and reasonable. Other backbones obtained relatively good results, implying that we can achieve excellent performance to some extent, demonstrating scalability.**

Table 5 Experimental results of BCINet based on different backbones.

Variants	mAcc	PixAcc	mIoU
Ours (MobileNet V2)	64.12	76.31	50.21
Ours (VGG16)	63.26	73.87	48.61
Ours (ResNet18)	65.05	75.45	50.35
Ours (ResNet101)	65.13	76.87	51.91
Ours (ResNet50)	**66.78**	**77.17**	**52.95**

5) A paper in ICCV21 called "ShapeConv: Shape-Aware Convolutional Layer for Indoor RGB-D Semantic Segmentation"is not referenced in this paper, which fails to achieve comparable results with compared methods. Is it due to the inconsistent baseline or some others reasons?

Response:

Thank you for your comments. In the revised manuscript, above-mentioned reference has been added and reviewed in Section 1, furthermore, the proposed BCINet has been compared with Reference [33] under the same conditions.

[33] J. Cao, H. Leng, D. Lischinski, D. Cohen-Or, C. Tu, and Y. Li, Shapeconv: Shape-aware convolutional layer for indoor RGB-D semantic segmentation. in Proceedings of the IEEE/CVF International Conference on Computer Vision (CVPR), 2021, pp. 7088–7097.

Highlights

1) Bilateral cross-modal interaction is achieved and hybrid contexts are exploited to improve segmentation accuracy.

2) A proposed FEM is embedded to highlight unimodally useful features.

3) An HPDC is designed to effectively collect diverse contextual information for improving the capability of BCINet.

4) A CGM is designed to transmit contextual information.

BCINet: Bilateral Cross-Modal Interaction Network for Indoor Scene Understanding in RGB-D Images

Wujie Zhou[a,b*], Yuchun Yue[a], Meixin Fang[b], Xiaohong Qian[a], Rongwang Yang[b], Lu Yu[b]

[a] *School of Information & Electronic Engineering, Zhejiang University of Science & Technology, Hangzhou 310023, China*

[b] *College of Information Science & Electronic Engineering, Zhejiang University, Hangzhou 310027, China*

Abstract

Depth cue has proven to be useful information in the indoor scene understanding of RGB-D images for providing a geometric counterpart to RGB representation. However, because of the differences between RGB-D image pairs, utilizing cross-modal data effectively is a key issue. Most methods exclusively leverage depth data to unilaterally complement RGB data for better feature representation; they invariably ignore the fact that RGB and depth data can bilaterally complement each other. Herein, a novel RGB-D scene-understanding network called BCINet is presented, in which RGB and depth data bilaterally complement each other via a proposed bilateral cross-modal interaction module (BCIM). The BCIM helps to capture cross-modal complementary cues by crossly fusing enhanced features from one modality to the counterpart modality through a feature enhanced module. Meanwhile, exploiting the long-range dependencies of RGB-D features is also significant for accurate scene understanding. Specifically, we design a hybrid pyramid dilated convolution module to enlarge the receptive fields along both the vertical and horizontal spatial directions to adaptively capture diverse contexts with different shapes. Additionally, we propose a context-guided module to aggregate these diverse higher-level contexts with lower-level features in the encoder to guide the information flow for progressively refining the segmentation map. Experimental results on two indoor scene datasets demonstrate the superiority and effectiveness of the proposed BCINet over several state-of-the-art approaches.

Keywords: Scene understanding, RGB-D, bilateral cross-modal interaction, hybrid pyramid dilated convolution, deep learning.

1. Introduction

Scene understanding aims to assign a category label to each pixel in an image; thus, it is a essential and fundamental machine vision task for many engineering applications such as video surveillance,

*Corresponding author.

E-mail addresses: wujiezhou@163.com

Postal address:310023

Tel.:+86-571-85070303.

medical image analysis [1, 2], robot perception [3], and, autonomous driving [4, 5]. RGB data contain rich appearance information and texture details, whereas depth data provide useful geometric cues for reliable segmentation of objects with ambiguous appearances [6]. With the development of range sensors (such as LiDAR and Kinect), depth data are applicable along with RGB images. By exploiting the two complementary modalities with a convolutional neural network (CNN) the scene-understanding performance can be improved.

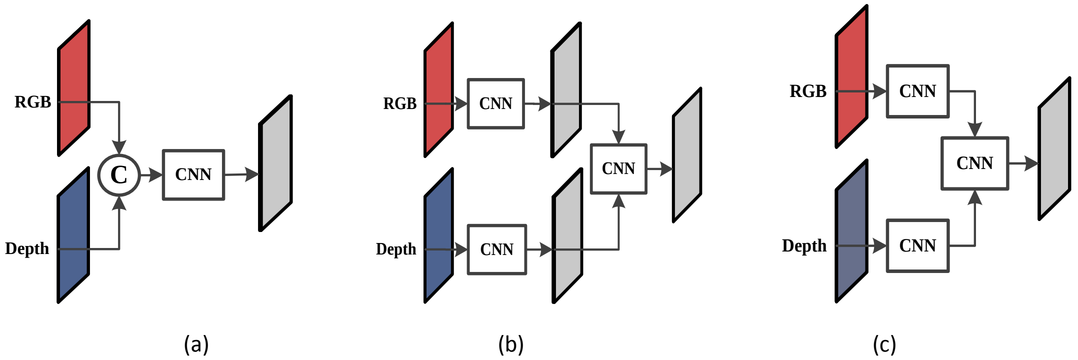

Fig. 1. Typical architectures to explore the relationship between an RGB image and depth map for scene understanding. (a) Concatenating RGB and depth channels, (b) fusing score maps computed from each modality, (c) sending RGB images and depth maps to two streams, then performing weighted fusion on the feature maps of both streams.

Concomitant with the success of vision recognition using CNNs, many scene-understanding approaches have adopted CNNs by extending them to pixel-wise classification. To solve the main problem of indoor scene understanding in RGB-D images of how to effectively extract and merge depth features along with RGB features, various methods have been presented that exploit the ability of CNNs for fusing depth data. The methods include concatenating the input RGB and depth streams, fusing score maps calculated from each modality, and sending RGB images and depth data to two streams, then performing weighted fusion on the feature maps of both streams, as shown in Figs. 1(a)–(c), respectively. Although these approaches achieve meaningful results, the correlation and interaction between RGB and depth data are only implicitly scrutinized. Furthermore, existing studies typically unilaterally assert that depth data are generally noisy, and may not lead to satisfactory results for scene understanding.

In contrast to the above assertion, we argue that the RGB image may also contain noisy features caused by the similar appearance of different neighboring objects, a possibility that is completely ignored by most studies. Neither RGB data nor depth data are completely flawless to their counterpart modality; they should be complemented with each other instead of only supplying depth map to RGB image data unilaterally. How to exploit the beneficial properties of the two types of data mutually and bilaterally is still rarely explored in existing studies.

Based on the above analysis, we propose a bilateral cross-modal interaction module (BCIM) to achieve bilateral interaction and to better exploit the relation between RGB and depth data. The key idea is to use a proposed feature enhanced module (FEM) to extract significant unimodal feature information by using attention mechanisms from both spatial-wise and channel-wise dimensions. Then, these unimodal useful features are crossly merged with their counterpart modal features. By merging discriminative features from the opposite modality, the BCIM facilitates bilateral cross-modal complementary information interaction without deteriorating modality-specific feature extraction, which promotes higher segmentation accuracy.

Simultaneously, context plays an important role in scene understanding, i.e., low-level contextual information could provide fine details for delineating the objects' boundary, whereas high-level contextual information describes the relationship between different parts and thus is extremely helpful for discovering the specific locations of objects. Diverse contexts contain more adaptive information of objects with irregular shapes in the complex indoor scenes. However, the issue of how to learn diverse contextual representation is still understudied in existing studies.

To explore more contexts for achieving high performance, atrous convolution [7] has proven highly effective in capturing contexts for classification tasks. However, a common limitation for regular dilated convolutions applied in atrous spatial pyramid pooling (ASPP) is that they all probe the input feature maps within square windows. This limits their flexibility in capturing anisotropic contexts that exist extensively in realistic scenarios. For example, the target objects may have a long-range strip structure in some cases, whether along the horizontal or vertical direction (e.g., the pillar and shelf in the first row of Fig. 2, the cabinet in the second row, and the pictures in the third row).

Merely using large square dilated convolution windows cannot adequately address this problem since it would incorporate contaminating cues from irrelevant regions [8]. Therefore, we propose a hybrid pyramid dilated convolution (HPDC) in this study, where we integrate rectangular dilated convolution into the common atrous convolution framework to collect more specific and diverse contexts apart from general contexts. The proposed HPDC deploys a long kernel shape along one spatial dimension with variable dilated rates but a narrow kernel shape along the other spatial dimension, which enables capturing of the long-range relationships of isolated regions, as shown in the third column of Fig. 2. This is essentially different from the traditional atrous convolution that only collects contextual information from a fixed square region, shown in the second column of Fig. 2. Furthermore, to successively propagate the diverse contexts collected by HPDC from higher to lower levels and effectively leverage the information of the encoder, we designed a context-guided module (CGM) in the decoder to harvest the flexible contexts of different levels.

The main contributions of this work are as follows:

1) A novel two-stream RGB-D scene-understanding network called BCINet is introduced, in which bilateral cross-modal interaction is achieved and hybrid contexts are exploited to improve segmentation accuracy.

2) A BCIM is introduced to bilaterally capture the cross-modal complementary cues between the unimodal RGB images and depth data, where a proposed FEM is embedded to highlight unimodally useful features.

3) An HPDC is designed to effectively collect diverse contextual information for improving the capability of BCINet to incorporate more anisotropic and characteristic features. A CGM is also designed to transmit contextual information collected by the HPDC from high levels to lower-level features for more diverse contextual exploration.

4) The proposed BCINet achieves state-of-the-art (SOTA) performances on two indoor scene datasets.

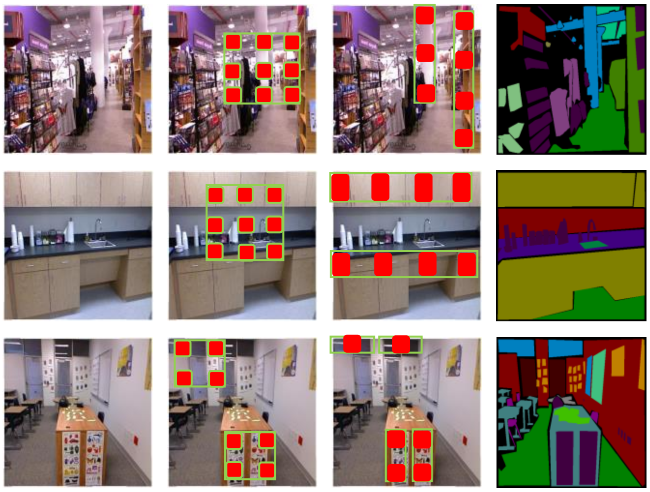

Fig. 2. Illustration of the difference between common dilated convolution and proposed HPDC for scene-understanding. The original RGB image, common dilated convolution operating on RGB, HPDC operating on RGB, and corresponding ground truth are displayed from left to right.

2. Related Work

2.1 RGB-D Scene Understanding

Recently, scene understanding based on fully convolutional networks [9] has achieved high performance. The introduction of the Microsoft Kinect sensor has significantly simplified the acquisition of depth data, and numerous segmentation methods based on RGB and depth modalities and their fusions have been developed. For instance, the methods in [10, 11] adopted an early fusion scheme for RGB and depth information for segmentation. Long *et al.* [9] used late fusion by adding the prediction results from the RGB and depth modalities. Peng *et al.* [12] directly concatenated RGB and depth data into a four-stream input to a multistage model. Nevertheless, the fusions in the aforementioned methods are mainly conducted by simple addition or concatenation; they fail to reflect the relations between RGB and depth data accurately.

To enhance fusions between the two types of data, subsequent methods more accurately exploit data relations. Han *et al.* [13] used a dual-channel late fusion network to integrate deep features from RGB and depth streams by appending a shared layer. Cheng *et al.* [14] adopted a gated fusion network to learn the varying contributions of each modality to determine categories in different scenes. Xiong *et al.* [15] presented a context-deformable variational model for adaptive receptive fields structured learning. Ma *et al.* [16] performed scene understanding by applying deep learning to RGB-D data in a multi-view context. Liu *et al.* [17] performed joint modeling by training a weighted sum model to fuse the features from two-stream deep CNNs using RGB and depth encoding. He *et al.* [18] provided a superpixel-based nerwork for scene understanding. First, region correspondences were computed from the optical flow and image boundary superpixels, and then a novel spatiotemporal pooling layer aggregated the corresponding information. Fayyaz *et al.* [19] included spatial and temporal features for scene understanding of street scenes by combining a long short-term memory (LSTM) network and a CNN. Liu *et al.* [20] introduced a fully connected continuous conditional random field (CRF) mdoule for continuous and discrete labeling. Lin *et al.* [21] considered depth cues to split an image into different layers with common characteristics regarding scenes/objects; a context-aware receptive field improved control of relevant contexts in the learned deep features. Wang *et al.* [22] proposed a depth-aware network comprising depth-aware average pooling and depth-aware convolutions. The scene geometry was seamlessly incorporated into the CNN by leveraging the depth similarity between pixels during information propagation. Yuan *et al.* [23] achieved indoor scene segmentation by incorporating RGB-D data and using a residual squeeze-and-excitation framework as an encoder to extract features from RGB-D data simultaneously. Then, feature fusion was performed during decoding. Lin *et al.* [24] introduced a switchable context model to facilitate RGB-D indoor scene-understanding. Their model analyzed the information in image regions to identify representative characteristics. Depth data allowed the identification of objects in these regions. Zhou *et al.* [25] performed indoor scene understanding using their three-branch self-attention framework that comprised two asymmetric input branches (i.e., asymmetric encoders) and a cross-modality distillation stream with a self-attention block. Wang *et al.* [26] used a feature transformation architecture to bridge deconvolutional and convolutional modules. They correlated the RGB and depth modalities by extracting common features; the modalities were characterized by specific features. Zhang *et al.* [27] proposed a multi-modality non-local aggregation network, which can effectively fuse non-local RGB-D feature maps along different dimensions. Li *et al.* [28] introduced the LSTM context fusion model to capture the context in RGB and depth streams by stacking an LSTM layer and several convolutional layers, respectively. Jiang *et al.* [29] presented a encoder–decoder residual framework for indoor scene understanding in RGB-D images. Qi *et al.* [30] introduced a graph neural module that builds a *KNN* graph on top of a point cloud. Lee *et al.* [31] presented a multimodality feature block and multilevel feature refinement block to fuse multilevel features through a top-down path. Similarly, Valada *et al.* [32] used self-supervised model adaptation fusion to combine modality-specific streams and fuse multilevel features through a top-down path. Cao *et al.* [33] proposed a shape-aware convolutional layer for indoor RGB-D scene-understanding.

Some methods consider depth information as an additional supervised signal to recalibrate RGB data in multitask learning. For instance, Zhang *et al.* [34] presented a pattern affinity propagation architecture to boost and regularize complementary tasks. Xu *et al.* [35] introduced a multimodality distillation module to pass valid information from depth data to RGB features. Chen *et al.* [36] presented an SA-Gate unit to guarantee cross-modality feature maps aggregation via an attention mechanism.

Although the abovementioned methods use complicated architectures and have notably advanced scene understanding, the novelty of our BCINet is that our model explicitly formulates bilateral interdependencies in a cross-modality framework without deteriorating modality-specific feature extraction, instead of unilaterally sending depth data to complement the RGB image or designing a complicated architecture to fuse the two types of data for a unified representation.

2.2 Attention Mechanisms

The attention mechanism resembling that of the human visual system has evolved along with some variants to perform many computer vision tasks. For instance, Chen *et al.* [37] used a cross-modality cross-level attention mechanism to aggregate useful cues from RGB and depth data while discarding redundant information. Zhang *et al.* [38] and Liu *et al.* [39] combined attention mechanisms with U-shaped models to guide feature integration. Yuan *et al.* and Fu *et al.* [40, 41] used self-attention block to obtain long-range contexts, obtaining a pixel-wise similarity results based on semantics pairs. Jia *et al.* [42] aggregated global contexts by learning a position-sensitive spatial attention mask to guide information flow. Wang *et al.* [43] introduced a non-local network for learning self-attention in 2D/3D vision modeling. Huang *et al.* [44] replaced a densely attention stream with a crisscross stream to enhance network efficiency. Cao *et al.* [45] unified the non-local architecture with SENet [46] to learn a global context using a lightweight architecture. Zhou *et al.* [47] presented a convolutional gated recurrent unit to extract valuable information iteratively from high levels while jointly using channel attention and spatial attention to distill discriminant cues from low levels. Hu *et al.* [48] introduced the attention complementary framework that gathers deep features from RGB-D data. Then, a channel-attention-based model extracts weighted features from these streams. Deng *et al.* [49] presented a residual fusion module with an attention mechanism. Zhang *et al.* [50] proposed an adaptive fusion module that explores the contributions of fused deep features at different levels to impede semantic dilution at high levels by applying feature-wise attention to learn weights exclusively. Zhou *et al.* [51] proposed a co-attention fusion method, which used an RGB feature query and a set of depth feature key–value pairs to transform the depth feature into the RGB feature space and then fuse with the local RGB features. Recently, the bidirectional-attention mechanism has been used for computer vision tasks such as depth estimation [52], object segmentation [53], object classification [54], and image-text matching [55].

In BCINet, we designed an FEM to highlight discriminative unimodal features through attention mechanisms. The FEM contains four parallel branches from both channel-wise and spatial-wise dimensions, each with a different focus.

2.3 Context Learning

Context plays a very important role in achieving high performance for various computer vision tasks. Many models are devoted to exploiting more discriminative contexts to improve their feature representation ability. Early techniques for modeling contextual relations for scene understanding involved CRFs [56, 57]. However, CRFs are mostly modeled in the discrete label, and thus are now less successful for producing SOTA results of scene parsing, even though they have been integrated into CNNs (strip pooling). Chen *et al.* [7] introduced an ASPP to capture multi-scale contexts for scene understanding. Zhao *et al.* [58] employed a pyramid pooling model to aggregate global and local contexts. Mei *et al.* [59] adopted two parallel context exploration (CE) blocks to perceive rich contextual information over a wide range of scales. Zhang *et al.* [60] proposed a multi-contextual module to distill features with different receptive fields and contextual characteristics. However, the ability of these methods to exploit contexts is limited because only the regular square kernel shapes are applied.

Our method differs from the above studies in that it explores diverse contextual information in an HPDC that integrates rectangular dilated convolutions into the common atrous convolution framework. The proposed HPDC module helps to enhance the discriminability of the framework via hybrid multi-scale contexts.

3. Proposed BCINet

3.1 Overview of the Architecture

Fig. 3 shows the framework of the proposed encoder–decoder BCINet, which takes RGB images and depth data as inputs and outputs the segmentation map in an end-to-end manner. The proposed BCINet is designed as an encoder–decoder architecture because that type of network is able to effectively obtain high-level semantic information as well as low-level detail information. For the encoder, we chose ResNet-50 [61] as the feature extractor for both the RGB and depth branches. After the RGB and depth data are fed into the two ResNet-50 branches, five levels of side-output feature maps of each modality are obtained, F_i^R for RGB images and F_i^D for depth data (i =1, 2, 3, 4, 5). At the first four stages of the RGB and depth branches, bilateral cross-modal feature interaction is achieved via the proposed BCIM, in which the proposed FEM is employed to exploit unimodally specific features, and these features are subsequently fused with the counterpart modal features. We fuse the features of each stage of both modalities by element-wise addition, denoted as $\{M_i \mid i = 1, 2, 3, 4, 5\}$, which are later fed to the CGM by skip connection. For the decoder part, the HPDC and CGM are employed in succession at each stage, where the HPDC module is first leveraged to explore diverse higher-level contextual information. The results and M_i are then jointly fed to the CGM to successively aggregate these diverse contexts with the lower-level features for better information flow. Finally, we use a convolution layer with a 3 × 3 kernel and an ensuing upsample operation on the feature maps of the last decoder to predict the final segmentation map.

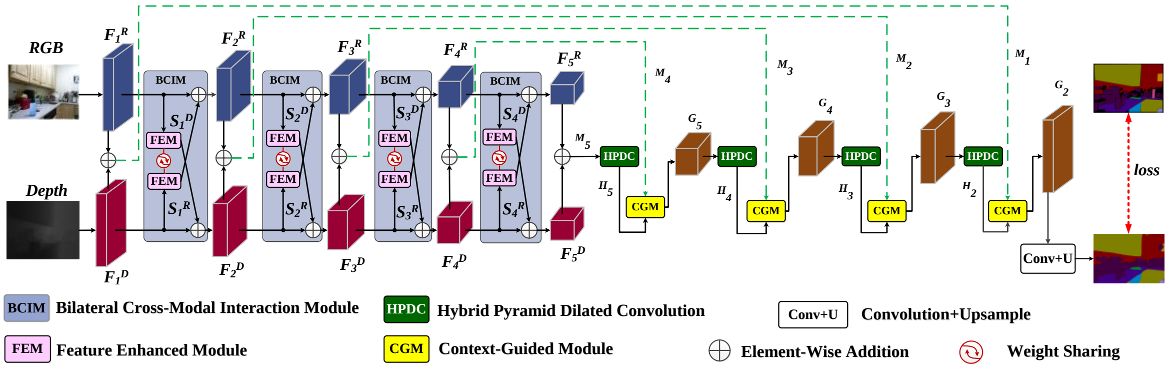
RGB
Depth
F1R
F1D
F2R
F2D
F3R
F3D
F4R
F4D
F5R
F5D
BCIM
FEM
S1D
S1R
S2D
S2R
S3D
S3R
S4D
S4R
M1
M2
M3
M4
M5
H2
H3
H4
H5
G2
G3
G4
G5
HPDC
CGM
Conv+U
loss
BCIM Bilateral Cross-Modal Interaction Module
FEM Feature Enhanced Module
HPDC Hybrid Pyramid Dilated Convolution
CGM Context-Guided Module
Conv+U Convolution+Upsample
Element-Wise Addition
Weight Sharing

Fig. 3. Overall architecture of the proposed BCINet for RGB-D indoor scene understanding.

3.2 *Bilateral Cross-Modal Interaction Module (BCIM)*

RGB-D scene understanding is a challenging computer vision task because there are large modality gaps between the RGB and depth data. Most existing methods unilaterally complement depth data to image data or simply fuse the unimodal RGB and depth features by concatenation and element-wise addition for capturing cross-modal information. Although these models may work well in some cases, they may produce some undesirable results when the relationships between RGB images and depth data are complicated. To solve this problem, a BCIM is presented, where we design an FEM to explore one-side unimodal enhanced features and then crossly feed them to the other-side unimodal features to achieve bilateral cross-modal interactions between both modalities.

The detailed framework of BCIM can be seen in Fig. 3, where each BCIM is shown as a light-blue block with two FEM submodules. Given the unimodal feature maps $F_i^R \in R^{C \times H \times W}$ and $F_i^D \in R^{C \times H \times W}$ at the i-th level (i = 1, 2, 3, 4), we utilize the FEM to extract unimodal distinguishing features S_i^R and S_i^D, respectively, for RGB and depth images (the visualization of learned modality-specific weights, S_i^R and S_i^D, is shown in Fig .4). Subsequently, these discriminative features are crossly merged into the counterpart modality by element-wise addition to obtain cross-modal features, which constitute the input to the next stage:

$$F_{i+1}^{R} = F_{i}^{R} + S_{i}^{D}, \quad i = 1, 2, 3, 4 \tag{1}$$

$$F_{i+1}^{D} = F_{i}^{D} + S_{i}^{R}, \quad i = 1, 2, 3, 4 \tag{2}$$

Both the RGB branch and depth branch adopt an FEM; meanwhile, the FEMs at the same stage applied in two modalities share the same weights, as shown in Fig. 3.

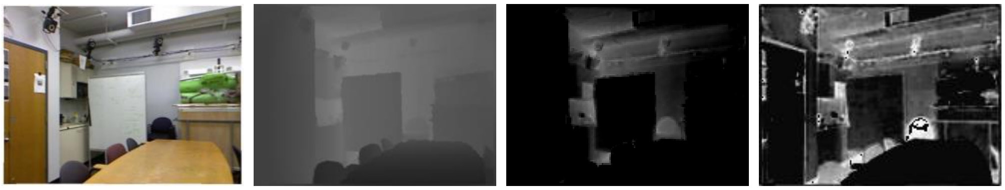
(a) RGB (b) Depth (c) S_i^R (c) S_i^D

Fig. 4 The visualization of learned modality-specific weights

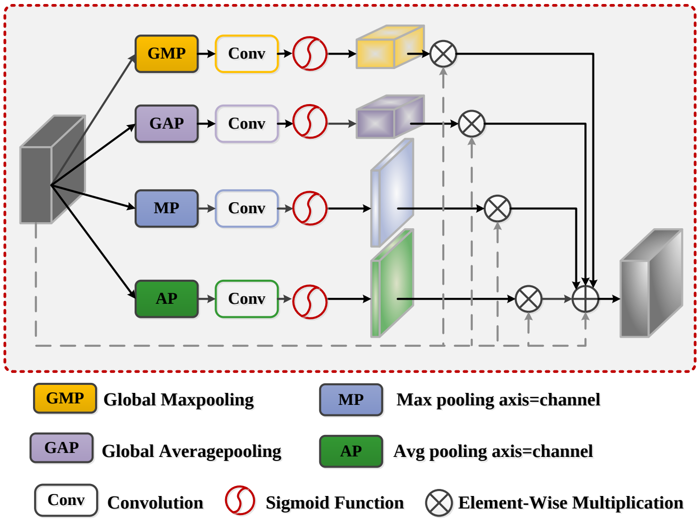
GMP
Conv
GAP
Conv
MP
Conv
AP
Conv
GMP Global Maxpooling
MP Max pooling axis=channel
GAP Global Averagepooling
AP Avg pooling axis=channel
Conv Convolution
Sigmoid Function
Element-Wise Multiplication

Fig. 5. Detailed structure of the proposed FEM.

The details of the FEM are presented in Fig. 5. Suppose that the input to the FEM is F_i^R; we design four parallel branches to highlight the distinguishing parts of the input features from both spatial-wise and channel-wise dimensions. The first two branches respectively perform global max pooling and global average pooling operations on the input features along the spatial direction. The results are subsequently sent to a 3 × 3 convolutional layer and a sigmoid function to obtain a channel-wise attention map. The channel-wise attention features are then pixel-wise multiplied with the input features to generate the channel weighted features. Similarly, the last two branches respectively perform max and average pooling operations on the input features along the channel direction, and are subsequently fed to a 3 × 3 convolutional layer and a sigmoid function to obtain spatial-wise attention features. The generated spatial attention maps are then pixel-wise multiplied with the input feature maps to obtain the spatially weighted feature maps. The above process can be formulated as follows:

$$\begin{cases} B_i^1 = \sigma(conv(GMP(F_i^R))) \times F_i^R \\ B_i^2 = \sigma(conv(GAP(F_i^R))) \times F_i^R \\ B_i^3 = \sigma(conv(MP(F_i^R))) \times F_i^R \\ B_i^4 = \sigma(conv(AP(F_i^R))) \times F_i^R \end{cases}, i = 1, 2, 3, 4 \tag{3}$$

where *GMP, GAP, MP,* and *AP* respectively represent global max pooling, global average pooling, max pooling, and average pooling. *Conv* denotes a 3 × 3 convolutional layer, *σ* denotes the sigmoid function, and × denotes pixel-wise multiplication. B_i^j is the result of the j-th branch (j = 1, 2, 3, 4) at the i-th level. The four enhanced features processed by each parallel branch are ultimately fused with the original input features by element-wise addition for better information incorporation:

$$S_i^R = B_i^1 + B_i^2 + B_i^3 + B_i^4 + F_i^R, \quad i = 1, 2, 3, 4 \tag{4}$$

Our FEM leverages four parallel branches to highlight the specific features of unimodality with each having a different focus, effectively enhancing the unimodal feature representation. With the proposed FEM embedded in the BCIM, bilateral interactions between unimodal RGB and depth feature maps are explored to capture effective cross-modal complementary cues, which explicitly formulate the correlations between the two types of data.

3.3 Hybrid Pyramid Dilated Convolution (HPDC) and Context-Guided Module (CGM)

The objects in indoor datasets may exhibit irregular scale changes. This necessitates features with diverse scale to cover the large-scale range for inferring various segmentation objects. Chen *et al.* [7] introduced an ASPP for generating multi-scale feature maps. More recently, Yang *et al.* [62] developed DenseASPP to densely cover the scale range by connecting atrous convolution layers in a dense manner [63]. Wang *et al.* [64] introduced a parallel ASPP module by imposing additional dilated convolutional layers into each dilated layer of the ASPP. Although these methods can obtain multi-scale feature maps that cover a large receptive field, their ability to exploit contexts is limited because only square kernel shapes are applied and they may unavoidably incorporate many irrelevant regions when processing objects with irregular shapes. Therefore, we propose an HPDC module to adaptively collect more diverse and anisotropic contextual information. Additionally, to connect the diverse contextual information with lower-level features in the encoder, we design a context-guided module (CGM) to progressively refine the segmentation map.

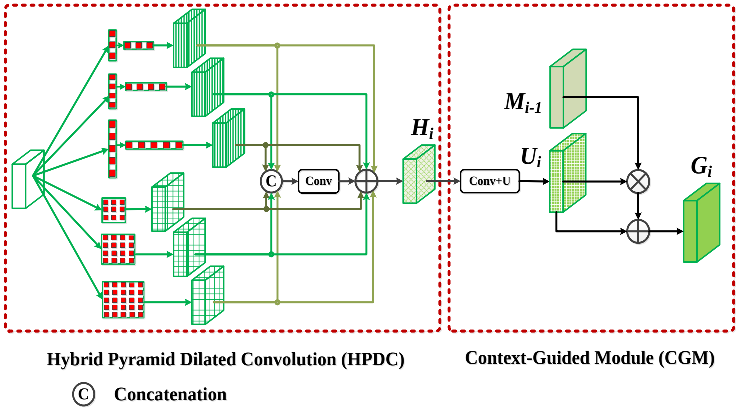
C
Conv
H_i
M_{i-1}
U_i
Conv+U
G_i
Hybrid Pyramid Dilated Convolution (HPDC)
Context-Guided Module (CGM)
Ⓒ Concatenation

Fig. 6. Detailed structure of the proposed HPDC and CGM.

As shown in the first half of Fig. 6, the HPDC consists of six parallel dilated convolutional branches with specific settings. Each of the first three branches adopts a kernel size of 1 × N and a following N

× 1 with dilation rates of *r*, 2*r*, and 3*r*, respectively, which are tailored to collect anisotropic contexts with irregular shapes. Concurrently, the other three parallel dilated convolutional branches with square kernel shapes are also applied to preserve the capability for common feature extractions. They adopt a unified kernel size of 3 × 3 and have dilated rates of *k*, 2*k*, and 3*k*, respectively. Suppose that the input of HPDC is *X*; the process can be formulated as follows:

$$\begin{cases} X_1 = Conv_{3\times1}^{r}(Conv_{1\times3}^{r}(X)) \\ X_2 = Conv_{5\times1}^{2r}(Conv_{1\times5}^{2r}(X)) \\ X_3 = Conv_{7\times1}^{3r}(Conv_{1\times7}^{3r}(X)) \\ X_4 = Conv_{3\times3}^{k}(X) \\ X_5 = Conv_{3\times3}^{2k}(X) \\ X_6 = Conv_{3\times3}^{3k}(X) \\ X_c = Cat(X_1, X_2, X_3, X_4, X_5, X_6) \end{cases} \tag{5}$$

where *Conv* represents the convolution with different kernel size, as illustrated by the subscripts in Eq. (5). *Cat* is the concatenation operation. The parameter N is set as 3, 5, and 7, respectively, for the first three branches; r is set as 2, 4, 4, and 2 and k is 6, 4, 2, and 1, respectively, for different levels of the decoder. Then, we apply a 1 × 1 convolution to squeeze the concatenation results to the same number as the input and they are further fused with the contextual features of the six parallel branches:

$$\begin{cases} T_i = \mathrm{Re}\,LU((BN(Conv_{1\times1}(X_c))) \\ H_i = T_i + X_1 + X_2 + X_3 + X_4 + X_5 + X_6 \end{cases} \quad i\text{=2, 3, 4, 5} \tag{6}$$

where *BN* denotes the batch normalization (BN) and *ReLU* is the activation function. H_i are the features output from the HPDC module, which are subsequently fed to the CGM, as displayed in the second half of Fig. 6. Mathematically, given H_i *and* M_{i-1}, the process of CGM is calculated by the following:

$$U_i = Up(\mathrm{Re}\,LU(BN(Conv_{1\times1}(H_i)))) \,, \quad i\text{=2, 3, 4, 5} \tag{7}$$

$$G_i = U_i \times M_{i-1} + U_i \,, \quad i\text{=2, 3, 4, 5} \tag{8}$$

where *Up* represents the upsample operation and G_i is the result output from CGM. With the proposed HPDC and CGM collaborating, more diverse and anisotropic contexts are exploited apart from the common contexts. Meanwhile, these higher-level contexts are fused with lower-level features in the encoder, achieving more robust and adaptive feature representation for better boundary delineation. The difference between our HPDC and the common ASPP is that we develop dilated rectangular convolutions with specific sizes to capture more anisotropic and diverse contexts, especially for those objects with irregular shapes. Simultaneously, the dilated rectangular convolutions we leverage can help to better cover the long dependencies along both the horizontal and vertical dimensions through our dilated settings, which is also different from the ordinary rectangular convolutions in some existing methods. The effectiveness of the design of our HPDC is validated in the ensuing ablation studies presented below.

4. Experimental Results

4.1 Datasets and Measures

To measure the prediction performance of our proposed BCINet, we conducted extensive experiments on two publicly used RGB-D scene-understanding datasets: NYUv2 [65] and SUN RGB-D [66]. The NYUv2 and SUN RGB-D (SUN for short) datasets contain 1,449 and 10,335 RGB-D images, respectively, and are divided into training and testing sets. We measured the proposed BCINet with existing SOTA approaches according to three measures: mean accuracy (mAcc.), pixel accuracy (PixAcc.), and mean intersection over union (mIoU).

4.2 Implementation Details

We implemented our proposed BCINet using the publicly available PyTorch library and executed it on an NVIDIA TITAN V GPU with 12 GB of memory in total. During training, we applied synchronous transforms to the inputs, including the RGB image, depth map, and corresponding annotations, for data augmentation. The operations included random flipping, random scaling, random cropping, random brightness adjustment, contrast adjustment, and saturation adjustment. We used ResNet-50s pre-trained on ImageNet [67] as our backbone in the encoder. The training and testing RGB-D images were resized to 480 × 640 resolutions. The SGD was applied as our optimizer, with weight decay 0.0005 and momentum 0.9. We used a batch size of 4/2 and trained the proposed BCINet for 150 and 100 epochs on the NYUv2 and SUN datasets, respectively. The learning rate was adjusted by the poly strategy [68] with a power of 0.9 and a basic learning rate of 0.005. We employed the cross-entropy loss function between the final predicted segmentation map and ground truth for end-to-end BCINet training. For the SUN dataset, when comparing with the SOTA models, we adopted flipping and multi-scale inference strategies for test-time augmentation and added the background as an additional weighted class during the training process to boost the performance.

4.3 Comparison with SOTA Methods

1) Quantitative Comparison on NYUv2 Dataset: We compared the experimental results of the proposed BCINet with those of the SOTA approaches in [9, 16–25, 33, 48, 51]. The experiments were conducted on the NYUv2 dataset. As illustrated in Table 1, we achieved superior results on the three evaluated measures. We attribute the better performance to the proposed BCIM, HPDC, and CGM, which respectively play a very important role in the accuracy of the entire framework. On the most important metric, mIoU, we achieved 52.95%—an approximately 0.55% improvement over the recent SOTA method by Chen *et al.* [36].

2) Quantitative Comparison on SUN Dataset: We performed additional experiments on the SUN dataset to examine the effectiveness and robustness of the proposed BCINet. The SUN dataset contains images from several different datasets. Compared with the NYUv2 dataset, the SUN dataset has more complex conditions and scenes, which we deemed suitable to evaluate the generality of

BCINet. From this dataset, we selected 5,285 RGB-D images for training and used the remaining RGB-D images for testing. We compared BCINet with the 13 SOTA scene-understanding methods in [6, 18, 21–22, 24, 27, 29–31, 33, 36, 51] on the SUN dataset. As shown in Table 2, BCINet outperformed the SOTA methods.

Table 1. Performance of different methods on the NYUv2 dataset. The best obtained result is highlighted.

Models	mAcc	PixAcc	mIoU
Long et al. [9]	46.1	65.4	34.0
Fayyaz *et al.* [19]	42.6	62.1	30.9
Liu *et al.* [20]	39.0	63.1	29.5
Ma *et al.* [16]	51.78	70.66	40.07
Liu *et al.* [17]	51.7	70.3	41.2
He *et al.* [18]	53.8	70.1	40.1
Wang *et al.* [22]	56.3	-	43.9
Lin *et al.* [21]	-	-	47.7
Yuan *et al.* [23]	59.27	74.42	46.79
Zhou *et al.* [25]	59.6	73.50	46.1
Hu *et al.* [48]	-	-	48.3
Xiong *et al.* [15]	63.5	-	50.7
Lin *et al.* [24]	-	-	50.7
Chen *et al.* [36]	-	**77.9**	52.4
Zhou *et al.* [51]	63.8	76.6	51.2
Zhang *et al.* [27]	-	**77.9**	52.3
Cao *et al.* [33]	63.5	76.4	51.3
Ours (ResNet-50)	**66.78**	77.17	**52.95**

Table 2. Performance of different models on the SUN dataset.

Models	mAcc	PixAcc	mIoU
Hazirbas *et al.* [6]	48.3	76.27	37.29
He *et al.* [18]	41.2	65.5	32.9
Wang *et al.* [22]	53.5	-	42.0
Jiang *et al.* [29]	60.3	81.3	47.8
Lin *et al.* [21]	-	-	48.1
Qi *et al.* [30]	57.0	-	45.9
Lee *et al.* [31]	60.1	81.5	47.7
Zhang *et al.* [27]	-	82.3	48.8
Chen *et al.* [36]	-	82.5	49.4
Hu *et al.* [48]	-	-	48.1
Zhou *et al.* [51]	60.5	82.5	49.3
Lin *et al.* [24]			49.5
Cao *et al.* [33]	59.2	82.2	48.6
Ours (ResNet-50)	**61.44**	**87.62**	**49.57**

3) Qualitative Comparison

To further demonstrate the predicted performance of the proposed BCINet, we conducted qualitative scene-understanding analyses by comparing BCINet with other methods [29, 31, 36, 48] and presented the scene-understanding results for a variety of indoor RGB-D images. Figure 7 shows the scene-understanding maps for RGB-D scenes obtained using NYUDv2, where BCINet obtained more accurate scene-understanding maps regardless of similar scenes or object size. Furthermore, the difference between similar categories is clearer. From these comparisons, we can conclude that BCINet not only accurately located the scene-understanding categories but also acquired detailed cues to recognize smooth objects.

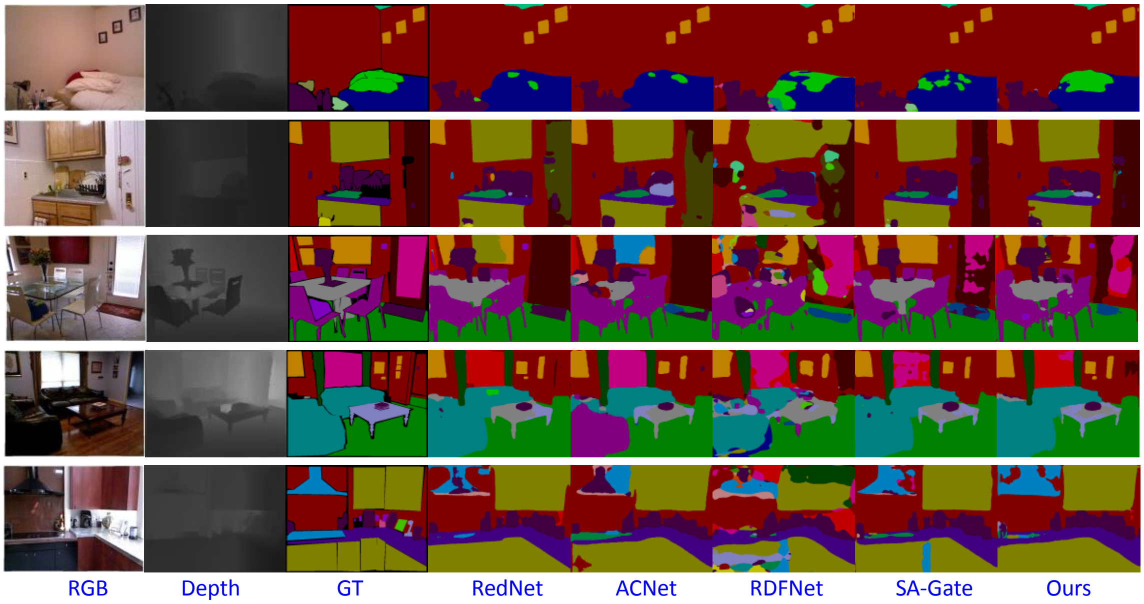

Fig. 7. Scene-understanding maps for RGB-D indoor scenes.

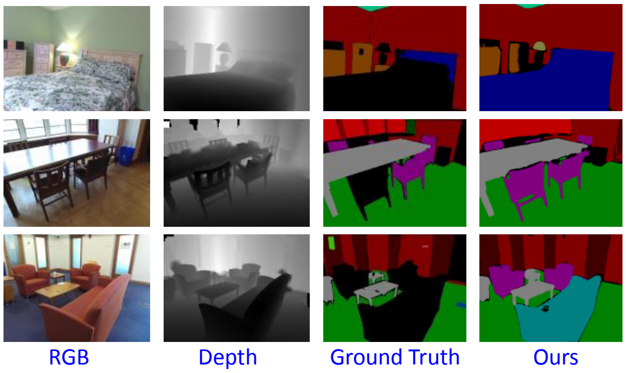

Fig. 8. Scene-understanding results from RGB-D images of the SUN test set.

Fig. 8 shows the scene-understanding results for RGB-D images using SUN. Some objects in SUN are mistakenly labeled as void, which is the background. Conversely, BCINet satisfactorily distinguishes such objects and shows good generalization. As shown in Fig. 8, some mistakes when labelling beds, chairs, and sofas exist. BCINet can correctly recognize these wrongly labeled objects using the information learned from other correctly labeled objects, demonstrating the superior performance of BCINet regarding complex objects and scenes.

4.4 Complexity Evaluation

Since runtime is an essential indicator of algorithm performance, we evaluated BCINet under the same conditions. We considered network inference time, number of floating-point operations, and parameter capacity as BCINet efficiency indicators—denoted as FPS, FLOPS, and Params, respectively.

To verify BCINet efficiency, we conducted extensive experiments and comparisons with SOTA RedNet [29], ACNet [48], RDFNet [31] and SA-Gate [36] models, as listed in Table 3. Therefore, the proposed BCINet is concluded to be an efficient network suitable for real-time applications.

Table 3. Efficiency measures on NYUv2 test set. FPS, FLOPS (G), and Params (M) represent network inference time, number of floating-point operations, and parameter capacity, respectively.

Models	Parameter(M)↓	FPS↑	Flops(G)↓
RedNet (ResNet50) [29]	82.0	26.5	101.8
ACNet (ResNet50) [48]	116.6	21.2	126.3
RDFNet (ResNet101) [31]	443.8	11.4	648.7
SA-Gate (ResNet101) [36]	110.6	16.6	176.5
Ours (ResNet50)	78.38	27.3	97.30

Table 4. Ablation study of each component of BCINet on the NYUv2 dataset.

Methods	mAcc	PixAcc	mIoU
w/o HPDC	62.87	75.28	49.14
w/o CGM	66.29	76.14	51.53
Only reconstruct the RGB branch	62.23	74.21	48.21
w/o BCIM	66.46	76.66	52.05
Remove FEM in BCIM	66.29	76.37	51.54
Replace FEM with self-attention	66.71	76.95	52.21
Replace HPDC with ASPP	66.73	77.05	52.36
BCINet	**66.78**	**77.17**	**52.95**

4.5 Ablation Studies

To verify the effectiveness of different modules in the proposed BCINet, several leave-one-out experiments were conducted on the NYUv2 dataset. The BCIM, HPDC, and CGM were first removed from the BCINet and replaced by their corresponding simpler techniques for scene understanding as the Baseline method. Specifically, the BCIM was replaced by element-wise addition to fuse multimodal feature maps and the CGM was replaced by a combination of simple convolutional (1 × 1) + BN + ReLU layer with successive upsampling operations for final segmentation inference. Then, as listed in Table 4, many versions of BCINet were designed for comparing the performance of BCINet with different experimental settings.

1) Effect of Backbone: To verify the influence of the backbone on BCINet, we compared the prediction performances of several other popular backbones (e.g., MobileNetV2, VGG16, and various ResNets with different sizes of parameter). Table 5 shows the experimental results. BCINet (ResNet50) obtained better performance compared with other backbones, indicating that our selection is desirable and reasonable. Other backbones obtained relatively good results, implying that we can achieve excellent performance to some extent, demonstrating scalability.

Table 5 Experimental results of BCINet based on different backbones.

Variants	mAcc	PixAcc	mIoU
Ours (MobileNet V2)	64.12	76.31	50.21
Ours (VGG16)	63.26	73.87	48.61
Ours (ResNet18)	65.05	75.45	50.35
Ours (ResNet101)	65.13	76.87	51.91
Ours (ResNet50)	**66.78**	**77.17**	**52.95**

2) Effect of BCIM and FEM: We designed the BCIM to explicitly model the complex relationships between RGB images and depth data by achieving bilateral cross-modal complementary information interaction. When we removed the BCIM from the whole framework, as shown in Table 4, the mIoU fell by 0.9%, verifying the effectiveness of our BCIM. Notably, if the FEM is removed from BCIM, the mIoU falls by 1.41%, which is worse than the results of removal of the whole BCIM. This indicates that inferior performance can result if we simply crossly fuse the original features of both modalities to each other without enhancing the feature correction. This substantiates our argument given in the Introduction and also validates the effectiveness of our FEM. For visualizations, as shown in the 4th column in Fig. 9, without BCIM, the model fails to obtain complementary cues, resulting in some objects with ambiguous appearance not being correctly classified. Additionally, owing to the lack of the FEM, the single modality discriminative features cannot be highlighted and extra noise is introduced, as can be seen in the 5th column. These situations are obviated when BCIM embedded with FEM is applied. In the third row of Fig. 9, although the blue striped area appears over the image without FEM, it does not appear in the one without BCIM, indicating more errors in the segmentation of other regions without FEM.

To validate the effectiveness of BCIM on transferring cross-modality information, a baseline with self-attention-based modules to enhance the unimodal representation learning has been added, as shown in Table 4. Although the experimental results of this method are lower than that of the proposed method, they are very competitive.

To validate the cross-modality data in the proposed method, we only reconstructed the RGB branch. This method only uses single mode features (without BCIM), and the experimental results are not particularly good.

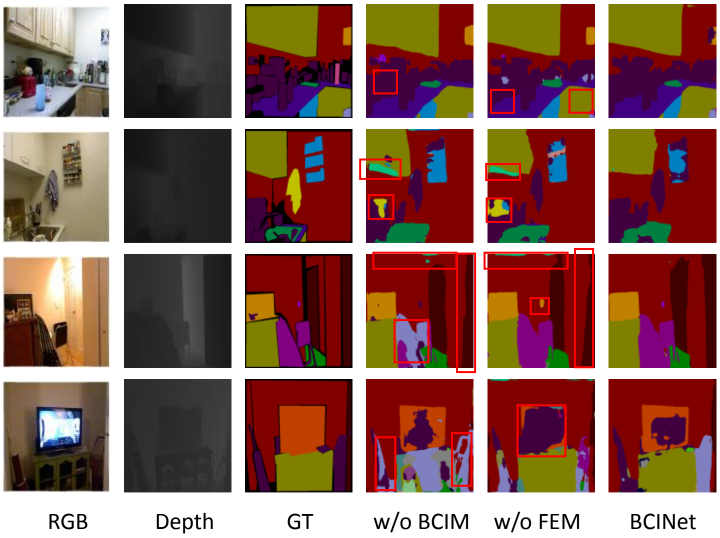

Fig. 9. Visualizations obtained by removing the BCIM and FEM.

3) Effect of HPDC: As can be seen in Table 4, the removal of HPDC causes a performance degradation of approximately 3.81%, which means that capturing diverse and anisotropic contexts plays a very important role in learning effective features. To verify the superiority of HPDC compared with the existing ASPP, we ablated HPDC by one more detailed experiment. As displayed in Table 4, when we replace our HPDC with common ASPP, the performance declines by 0.58%, indicating that the three branches that adopt dilated rectangular convolutions in HPDC yield extra gains. As shown in the third row of Fig. 10, although the quilt is better parsed with ASPP, some additional errors in the segmentation of other regions with ASPP exist. As shown in the 4th column in Fig. 10, when HPDC is removed, the model fails to formulate long dependencies and large-scale variations between objects. Furthermore, if the HPDC is replaced by ASPP, objects with irregular shapes cannot be well segmented or correctly classified, which proves the effectiveness of the design of our HPDC.

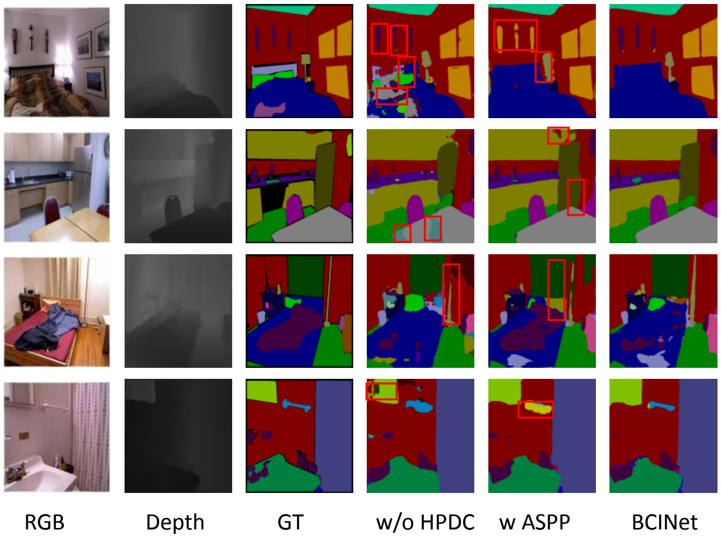

Fig. 10. Visualizations obtained by removing the HPDC and replacing HPDC with ASPP.

4) Effect of CGM: Clearly, the performance falls by 1.42% when CGM is not used. This indicates that CGM can better refine cross-modal high-level features by using the diverse contexts of higher levels to guide the fusion of cross-modal lower-level feature maps in the encoder in a cascaded manner. As shown in the 4th column in Fig. 11, adding CGM results in better boundary delineation and higher accuracy for small objects.

Overall, Baseline + BCIM + HPDC + CGM yields the best performance of 52.95%, representing a 6.37% gain over the Baseline model. This implies that, with the collaboration of the BCIM, HPDC, and CGM, bilateral cross-modal complementary information is effectively obtained and diverse contexts are comprehensively exploited to improve the scene-understanding performance.

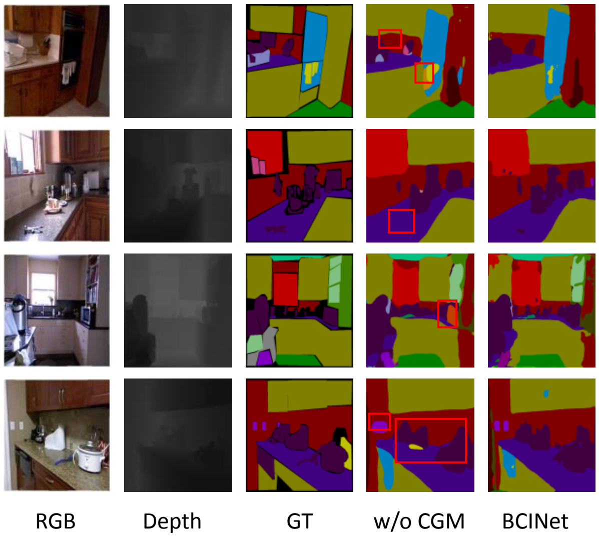

Fig. 11. Visualizations obtained by removing the CGM.

5. Conclusion

In this study, we proposed BCINet—which comprises BCIM, HPDC, and CGM—for RGB-D indoor scene understanding. BCIM executes bilateral fusion strategies to achieve more effective cross-modal information interaction while preserving modality-specific features. HPDC is designed to capture more diverse and anisotropic contexts to adapt large-scale variations and objects with irregular shapes in indoor datasets. CGM guides the abundant and diverse high-level contexts captured by HPDC to aggregate them with lower-level features in the encoder, which facilitates boundary delineation and segmentation refinement. The results of experiments conducted on the NYUv2 and SUN datasets indicate that the proposed BCINet outperforms SOTA RGB-D scene-understanding models. In the future, we will continue improving BCINet and attempt to apply it to other computer vision tasks, such as outdoor RGB-D crowd counting and RGB-thermal scene-understanding.

Acknowledgements

This work was supported by National Natural Science Foundation of China (61502429, 61672337, 61972357); the Zhejiang Provincial Natural Science Foundation of China (LY18F020012, LY17F020011); and Zhejiang Key R & D Program (2019C03135).

References

1. Y. Wang, W. Song, G. Fortino, L. -Z. Qi, W. Zhang and A. Liotta, Underwater images: An Experimental-Based Review of Image Enhancement and Image Restoration Methods for Underwater Imaging, IEEE Access, 7, (2019) 140233–140251.
2. H. Xu, and J. Ma, EMFusion: An unsupervised enhanced medical image fusion network. Information Fusion, 76, (2021) 177–186.
3. I. Ahmed, S. Din, G. Jeon, F. Piccialli and G. Fortino, Collaborative robotics: Towards Collaborative Robotics in Top View Surveillance: A Framework for Multiple Object Tracking by Detection Using Deep Learning, IEEE CAA J. Autom. Sinica, 8, (2021) 1253–1270.
4. K. Lin, Y. Li, J. Sun, D. Zhou, and Q. Zhang, Multi-sensor fusion for body sensor network in medical human–robot interaction scenario. Information Fusion, 57, (2020) 15–26.
5. G. Fortino, C. Savaglio, G. Spezzano and M. Zhou, IoT: Internet of Things as System of Systems: A Review of Methodologies, Frameworks, Platforms, and Tools, IEEE Trans. Syst. Man Cybern. Syst., 51, (2021) 223–236.
6. C. Hazirbas, L. Ma, C. Domokos, and D. Cremers, FuseNet: Incorporating depth into semantic segmentation via fusion-based CNN architecture, in Proceedings of Asian Conference on Computer Vision (ACCV), 2016, pp. 213–228.
7. L.-C. Chen, G. Papandreou, I. Kokkinos, K. Murphy, and A. L. Yuille, Deeplab: Semantic image segmentation with deep convolutional nets, atrous convolution, and fully connected crfs, IEEE Transactions on Pattern Analysis and Machine Intelligence, 40, (2018) 834–848.
8. J. He, Z. Deng, L. Zhou, Y. Wang and Y. Qiao, Adaptive Pyramid Context Network for Semantic Segmentation, in Proceedings of the IEEE/CVF Conference on Computer Vision and Pattern Recognition (CVPR), 2019, pp. 7511–7520.
9. J. Long, E. Shelhamer, and T. Darrell, Fully Convolutional Networks for Semantic Segmentation, in Proceedings of the IEEE/CVF Conference on Computer Vision and Pattern Recognition (CVPR), 2015, pp. 3431–3440.
10. H. Zhao, J. Shi, X. Qi, X. Wang, and J. Jia, Pyramid Scene Parsing Network, in Proceedings of the IEEE/CVF Conference on Computer Vision and Pattern Recognition (CVPR), 2017, pp. 2881–2890.
11. C. Couprie, C. Farabet, L. Najman, and Y. Lecun, Indoor Semantic Segmentation using depth information, 2013, [Online] Available: https://arxiv.org/pdf/1301.3572.
12. H. Peng, B. Li, W. Xiong, W. Hu, and R. Ji, RGBD salient object detection: A benchmark and algorithms, in Proceedings of the European Conference on Computer Vision(ECCV), 2014, pp. 92-109.
13. J. Han, H. Chen, N. Liu, C. Yan and X. Li, CNNs-Based RGB-D Saliency Detection via Cross-View Transfer and Multiview Fusion, IEEE Transactions on Cybernetics, 48, (2018) 3171–3183.
14. Y. Cheng, R. Cai, Z. Li, X. Zhao and K. Huang, Locality-Sensitive Deconvolution Networks with Gated Fusion for RGB-D Indoor Semantic Segmentation, in Proceedings of the IEEE/CVF Conference on Computer Vision and Pattern Recognition (CVPR), 2017, pp. 1475–1483.
15. Z. Xiong, Y. Yuan, N. Guo and Q. Wang, Variational Context-Deformable ConvNets for Indoor Scene Parsing, in Proceedings of

the IEEE/CVF Conference on Computer Vision and Pattern Recognition (CVPR), 2020, pp. 3991–4001.

16. L. Ma, J. Stückler, C. Kerl and D. Cremers, Multi-view deep learning for consistent semantic mapping with RGB-D cameras, in Proceedings of the IEEE/RSJ International Conference on Intelligent Robots and Systems (IROS), 2017, pp. 598–605.

17. H. Liu, W. Wu, X. Wang, and Y. Qian, RGB-D joint modelling with scene geometric information for indoor semantic segmentation, Multimedia Tools and Applications, 77, (2018) 22475–22488.

18. Y. He, W. Chiu, M. Keuper and M. Fritz, STD2P: RGBD Semantic Segmentation Using Spatio-Temporal Data-Driven Pooling, in Proceedings of the IEEE Conference on Computer Vision and Pattern Recognition (CVPR), 2017, pp. 7158–7167.

19. M. Fayyaz, M. H. Saffar, M. Sabokrou, M. Fathy, F. Huang, and R. Klette, STFCN: Spatio-temporal fully convolutional neural network for semantic segmentation of street scenes, in Proceedings of Asian Conference on Computer Vision(ACCV), 2016, pp. 493–509.

20. F. Liu, G. Lin and C. Shen, Discriminative Training of Deep Fully Connected Continuous CRFs With Task-Specific Loss, IEEE Transactions on Image Processing, 26, (2017) 2127–2136.

21. D. Lin, G. Chen, D. Cohen-Or, P. Heng and H. Huang, Cascaded Feature Network for Semantic Segmentation of RGB-D Images, in Proceedings of the IEEE/CVF International Conference on Computer Vision (ICCV), 2017, pp. 1320–1328.

22. W. Wang and U. Neumann, Depth-aware CNN for RGB-D Segmentation, in Proceedings of the European Conference on Computer Vision(ECCV), 2020, pp. 135–150.

23. J. Yuan, W. Zhou and T. Luo, DMFNet: Deep Multi-Modal Fusion Network for RGB-D Indoor Scene Segmentation, IEEE Access, 7, (2019) 169350–169358.

24. D. Lin, R. Zhang, Y. Ji, P. Li and H. Huang, SCN: Switchable Context Network for Semantic Segmentation of RGB-D Images, IEEE Transactions on Cybernetics, 50, (2020) 1120–1131.

25. W. Zhou, J. Yuan, J. Lei and T. Luo, TSNet: Three-stream Self-attention Network for RGB-D Indoor Semantic Segmentation, IEEE Intelligent Systems, 36, (2021) 73–78.

26. J. Wang, Z. Wang, D. Tao, S. See, and G. Wang, Learning common and specific features for RGB-D semantic segmentation with deconvolutional networks, in Proceedings of the European Conference on Computer Vision(ECCV), 2016, pp. 664–679.

27. G. Zhang, J. -H. Xue, P. Xie, S. Yang and G. Wang, Non-Local Aggregation for RGB-D Semantic Segmentation, IEEE Signal Processing Letters, 28, (2021) 658–662.

28. Z. Li, Y. Gan, X. Liang, Y. Yu, H. Cheng, and L. Lin, LSTM-CF: Unifying context modeling and fusion with LSTMs for RGB-D scene labeling, in Proceedings of the European Conference on Computer Vision(ECCV), 2016, pp. 541–557.

29. J. Jiang, L. Zheng, F. Luo, and Z. Zhang, RedNet: Residual encoder-decoder network for indoor RGB-D semantic segmentation, 2018, [Online] Available: https://arxiv.org/pdf/1806.01054.

30. X. Qi, R. Liao, J. Jia, S. Fidler and R. Urtasun, 3D Graph Neural Networks for RGBD Semantic Segmentation, in Proceedings of the IEEE/CVF International Conference on Computer Vision (ICCV), 2017, pp. 5209–5218.

31. S. Lee, S. Park and K. Hong, RDFNet: RGB-D Multi-level Residual Feature Fusion for Indoor Semantic Segmentation, in Proceedings of the IEEE/CVF International Conference on Computer Vision (ICCV), 2017, pp. 4990–4999.

32. A. Valada, R. Mohan, and W. Burgard, Self-Supervised Model Adaptation for Multimodal Semantic Segmentation, International Journal of Computer Vision, 128, (2020) 1239–1285.

33. J. Cao, H. Leng, D. Lischinski, D. Cohen-Or, C. Tu, and Y. Li, Shapeconv: Shape-aware convolutional layer for indoor RGB-D semantic segmentation. in Proceedings of the IEEE/CVF International Conference on Computer Vision (CVPR), 2021, pp.

7088–7097.

34. Z. Zhang, Z. Cui, C. Xu, Y. Yan, N. Sebe and J. Yang, Pattern-Affinitive Propagation Across Depth, Surface Normal and Semantic Segmentation, in Proceedings of the IEEE/CVF Conference on Computer Vision and Pattern Recognition (CVPR), 2019, pp. 4101–4110.
35. D. Xu, W. Ouyang, X. Wang and N. Sebe, PAD-Net: Multi-tasks Guided Prediction-and-Distillation Network for Simultaneous Depth Estimation and Scene Parsing, in Proceedings of the IEEE/CVF Conference on Computer Vision and Pattern Recognition(CVPR), 2018, pp. 675–684.
36. X. Chen, K. Lin, J. Wang, W. Wu, C. Qian, H. Li, and G. Zeng, Bi-directional Cross-Modality Feature Propagation with Separation-and-Aggregation Gate for RGB-D Semantic Segmentation, 2020, [Online] Available: https://arxiv.org/pdf/2007.09183.
37. H. Chen and Y. Li, Three-Stream Attention-Aware Network for RGB-D Salient Object Detection, IEEE Transactions on Image Processing, 28, (2019) 2825–2835.
38. X. Zhang, T. Wang, J. Qi, H. Lu and G. Wang, Progressive Attention Guided Recurrent Network for Salient Object Detection, in Proceedings of the IEEE/CVF Conference on Computer Vision and Pattern Recognition (CVPR), 2018, pp. 714–722.
39. N. Liu, J. Han and M. Yang, PiCANet: Learning Pixel-Wise Contextual Attention for Saliency Detection, in Proceedings of the IEEE/CVF Conference on Computer Vision and Pattern Recognition (CVPR), 2018, pp. 3089–3098.
40. J. Fu, J. Liu, H. Tian, Y. Li, Y. Bao, Z. Fang and H. Lu, Dual Attention Network for Scene Segmentation, in Proceedings of the IEEE/CVF Conference on Computer Vision and Pattern Recognition (CVPR), 2019, pp. 3141–3149.
41. Y. Yuan and J. Wang, OCNet: Object context network for scene parsing, 2018, [Online] Available: https://arxiv.org/pdf/1809.00916.
42. J. Jia, PSANet: Point-wise Spatial Attention Network for Scene Parsing, in Proceedings of the European Conference on Computer Vision (ECCV), 2018, pp. 267–283.
43. X. Wang, R. Girshick, A. Gupta, and K. He, Non-local Neural Networks, in Proceedings of the IEEE/CVF Conference on Computer Vision and Pattern Recognition (CVPR), 2018, pp. 7794–7803.
44. Z. Huang, X. Wang, L. Huang, C. Huang, Y. Wei and W. Liu, CCNet: Criss-Cross Attention for Semantic Segmentation, in Proceedings of the IEEE/CVF International Conference on Computer Vision (ICCV), 2019, pp. 603–612.
45. Y. Cao, J. Xu, S. Lin, F. Wei and H. Hu, GCNet: Non-Local Networks Meet Squeeze-Excitation Networks and Beyond, in Proceedings of the IEEE/CVF International Conference on Computer Vision Workshop (ICCVW), 2019, pp. 1971–1980.
46. J. Hu, L. Shen, S. Albanie, G. Sun and E. Wu, Squeeze-and-Excitation Networks, in Proceedings of the IEEE/CVF Conference on Computer Vision and Pattern Recognition (CVPR),, 2018, pp. 7132–7141.
47. Z. Zhou, Z. Wang, H. Lu, S. Wang, and M. Sun, Multi-Type Self-Attention Guided Degraded Saliency Detection, in Proceedings of the AAAI Conference on Artificial Intelligence, 2020, pp. 13082–13089.
48. X. Hu, K. Yang, L. Fei and K. Wang, ACNET: Attention Based Network to Exploit Complementary Features for RGBD Semantic Segmentation, in Proceedings of the IEEE International Conference on Image Processing (ICIP), 2019, pp. 1440–1444.
49. L Deng, M Yang, T Li, Y He and C Wang, RFBNet: deep multimodal networks with residual fusion blocks for RGB-D semantic segmentation, 2019, [online] Available:https://arxiv.org/pdf/1907.00135.
50. M. Zhang, Y. Zhang, Y. Piao, B. Hu and H. Lu, Feature Reintegration over Differential Treatment: A Top-down and Adaptive Fusion Network for RGB-D Salient Object Detection, in Proceedings of the 28th ACM International Conference on Multimedia,

2020, pp. 4107–4115.

51. H. Zhou, L Qi, Z Wan, H Huang and X. Yang, RGB-D Co-attention Network for Semantic Segmentation, in Proceedings of Asian Conference on Computer Vision(ACCV), 2020, pp. 519–536.

52. S. Aich, J. M. U. Vianney, M. A. Islam, and M. K. B. Liu, Bidirectional attention network for monocular depth estimation, In 2021 IEEE International Conference on Robotics and Automation (ICRA), (2021) 11746–11752.

53. G. P. Ji, K. Fu, Z. Wu, D.-P. Fan, J. Shen, and L. Shao, Full-duplex strategy for video object segmentation. In Proceedings of the IEEE/CVF International Conference on Computer Vision, (2021) 4922–4933.

54. C. Liu, H. Xie, Z. Zha, L. Yu, Z. Chen, and Y. Zhang, Bidirectional attention-recognition model for fine-grained object classification. IEEE Transactions on Multimedia, 22(7), (2019) 1785–1795.

55. C. Liu, Z. Mao, A. A. Liu, T. Zhang, B. Wang, and Y. Zhang, Focus your attention: A bidirectional focal attention network for image-text matching. In Proceedings of the 27th ACM International Conference on Multimedia, 2019, pp. 3–11.

56. R. Vemulapalli, O. Tuzel, M. Liu and R. Chellappa, Gaussian Conditional Random Field Network for Semantic Segmentation, in Proceedings of the IEEE/CVF Conference on Computer Vision and Pattern Recognition (CVPR), 2016, pp. 3224-3233.

57. S. Zheng, S. Jayasumana, B. Romera-Paredes, V.Vineet, Z. Su, D. Du, C. Huang and P. H. S. Torr, Conditional Random Fields as Recurrent Neural Networks, in Proceedings of the IEEE/CVF International Conference on Computer Vision (ICCV), 2015, pp. 1529-1537.

58. H. Zhao, J. Shi, X. Qi, X. Wang, and J. Jia, Pyramid scene parsing network, in Proceedings of the IEEE/CVF Conference on Computer Vision and Pattern Recognition (CVPR), 2017, pp. 2881–2890.

59. H. Mei, G. Ji, Z. Wei, X. Yang, X. Wei, and D. Fan, Camouflaged object segmentation with distraction mining, in Proceedings of the IEEE/CVF Conference on Computer Vision and Pattern Recognition (CVPR), 2021, pp. 8772-8781.

60. J. Zhang, C. Long, Y. Wang, X. Yang, H. Mei, and B. Yin, Multicontext and enhanced reconstruction network for single image super resolution, in Proceedings of the IEEE International Conference on Multimedia and Expo(ICME), 2020, pp. 1–6.

61. K. He, X. Zhang, S. Ren and J. Sun, Deep Residual Learning for Image Recognition, in Proceedings of the IEEE/CVF Conference on Computer Vision and Pattern Recognition (CVPR), 2016, pp. 770-778.

62. M. Yang, K. Yu, C. Zhang, Z. Li, and K. Yang, DenseASPP for semantic segmentation in street scenes, in Proceedings of the IEEE/CVF Conference on Computer Vision and Pattern Recognition (CVPR), 2018, pp. 3684–3692.

63. G. Huang, Z. Liu, L. Van Der Maaten, and K. Q. Weinberger, Densely connected convolutional networks, in Proceedings of the IEEE/CVF Conference on Computer Vision and Pattern Recognition (CVPR), 2017, pp. 4700–4708.

64. L. Wang, R. Chen, L. Zhu, H. Xie and X. Li, Deep Sub-Region Network for Salient Object Detection, IEEE Transactions on Circuits and Systems for Video Technology, 31 (2021) 728–741.

65. N. Silberman, D. Hoiem, P. Kohli, and R. Fergus, Indoor segmentation and support inference from RGBD images, in Proceedings of the European Conference on Computer Vision(ECCV), 2012, pp. 746–760.

66. S. Song, S. P. Lichtenberg and J. Xiao, SUN RGB-D: A RGB-D scene understanding benchmark suite, in Proceedings of the IEEE/CVF Conference on Computer Vision and Pattern Recognition (CVPR), 2015, pp. 567–576.

67. J. Deng, W. Dong, R. Socher, L. Li, Kai Li, and Li Fei-Fei, Imagenet: A large-scale hierarchical image database, in Proceedings of the IEEE/CVF Conference on Computer Vision and Pattern Recognition (CVPR), 2009, pp. 248–255.

68. W. Liu, A. Rabinovich, and A. C. Berg, Parsenet: Looking wider to see better, 2015, [online] Available:https://arxiv.org/pdf/1506.04579